UAS in MIKE

Underwater Acoustic Simulation Module

Scientific Documentation

DHI A/S headquarters
Agern Allé 5
DK-2970 Hørsholm
Denmark

+45 4516 9200 Telephone
+45 4516 9333 Support
+45 4516 9292 Telefax

mike@dhigroup.com
www.mikepoweredbydhi.com

PLEASE NOTE

CONTENTS

UAS in MIKE
Underwater Acoustic Simulation Module
Scientific Documentation

1 Introduction

The present underwater acoustic model developed by DHI focuses on the noise propagation in the far-field with the aim of providing a basis for conducting a risk assessment of environmental noise impacts. The sources of sound that may affect the surrounding marine life may be noise emanating from pile driving related to offshore wind turbine installation, dredging, seismic survey, ship propulsion, etc.

A very effective and popular wave-theory technique for solving range-dependent[1] propagation problems in ocean acoustics is the parabolic equation method (Tappert, 1977). The method requires environments slowly varying with range and azimuth and that a preferred direction of propagation exists. Two criteria that underlie the widespread use of parabolic approximations in this context are: (1) outgoing energy dominates over backscattered energy, hence backscattering in the far-field is negligible, and (2) long-range sound propagation in the ocean waveguide is dominated by energy travelling at small angles to the horizontal. A noise source is often of spherical nature in the near field, however, as the acoustic waves propagate further away the wave fronts become cylindrical as they are confined between the seabed and water surface - further supporting a 2D modelling approach.

The present model is based on solving the Parabolic Equation (PE). The governing wave equation of parabolic nature is derived from the Helmholtz equation. There exists an infinity of parabolic approximations to this three-dimensional, elliptic partial differential equation, and the **U**nderwater **A**coustic **S**imulator (UAS) in MIKE is based on the 2D, very-wide angle formulation by Collins (1989). The very-wide angle approximation is important for propagation very near the source and propagation out to very long ranges.

Collins (1993) further refined his higher-order PE formulation based on a Padé series by a split-step Padé solution for the PE method. The paper was complemented by a corresponding algorithm of the split-step Padé solution, which forms the basis for UAS. The RAM[2] algorithm is outlined in Collins (1999a). By applying a higher-order Padé approximation (leading to higher-order PE) both numerical errors and asymptotic errors (e.g. phase errors due to wide-angle propagation) are reduced, and at the same time high computational efficiency is achieved. The splitting solution requires the numerical solution of the governing equation for each term of the Padé approximation.

The principal advantage of the parabolic wave equation over the elliptic Helmholtz equation is that the PE is a one-way wave equation (first-order in range) which can be solved by a range-marching solution technique - step by step from the source. The PE method is based on factoring the operator in the frequency-domain wave equation in order to obtain an outgoing wave equation. With this follows requirements of specification of both initial and boundary conditions for the ocean environment considered. In other words, the one-way wave equation for the envelope of the acoustic pressure implies numerically solving an initial value problem instead of an elliptic boundary value problem.

The original split-step Padé solution accounts for attenuation in the seabed. Volume attenuation[3] in the water column has a significant impact on sound wave propagation of

[1] Situations where the lateral variability along the propagation path strongly influences the acoustic sound field pattern. Environmental parameters such as sound-speed profile, water depth, and bottom composition are not invariant with range.

[2] Range-dependent Acoustic Model

[3] Volume attenuation of sound in seawater is governed by viscosity, temperature, pressure, salinity, and acidity (pH value).

above 1 kHz (Ainslie 2010) and is important to take into account when modelling broad band noise. The split-step Padé solution algorithm was expanded to consider the attenuation of acoustic waves in water. UAS includes propagation in the seabed, but handles only compressional waves and not shear waves, i.e. ocean bottom sediments are modelled as fluids.

The original paper by Collins (1993) describing the split-step Padé solution and the paper outlining part of the finite difference discretisation used (Collins, 1989) are both referenced in Chapter 4.

2 Parabolic Equation Technique

The core of the UAS is a 2D (vertical) range-dependent acoustic model simulating transmission loss (TL) in a vertical transect (r-z plane) for a given omnidirectional sound source located at the start of the transect and ambient conditions. UAS allows for simulating the effect of a noise source with broad band signature.

At a certain distance from the source, the complex pressure, p, satisfies the following far-field equation in each 2D range-independent region (Collins, 1993;1999a):

$$\frac{\partial^2 p}{\partial r^2} + \rho \frac{\partial}{\partial z}\left(\frac{1}{\rho}\frac{\partial p}{\partial z}\right) + k^2 p = 0 \tag{2.1}$$

where ρ is the density, $k = (1 + i\eta\beta)\omega/c$ is the wave number, i is the imaginary unit, ω is the circular frequency, c is the sound speed, β is the attenuation in dB per wave length, and $\eta = (40\pi \log_{10} e)^{-1}$. Factoring the operator in Eq. (2.1) will result in:

$$\left(\frac{\partial}{\partial r} + ik_0(1+X)^{1/2}\right)\left(\frac{\partial}{\partial r} - ik_0(1+X)^{1/2}\right)p = 0 \tag{2.2}$$

$$X = k_0^{-2}\left(\rho \frac{\partial}{\partial z}\frac{1}{\rho}\frac{\partial}{\partial z} + k^2 - k_0^2\right) \tag{2.3}$$

with $k_0 = \omega/c_0$ and c_0 as the representing phase speed. Assuming that the outgoing energy is dominating the back-scattered energy, the outgoing wave equation can be written as:

$$\frac{\partial p}{\partial r} = ik_0(1+X)^{1/2}p \tag{2.4}$$

The formal solution of Eq. (2.4) is:

$$p(r + \Delta r, z) = exp\left(ik_0 \Delta r(1+X)^{1/2}\right)p(r,z) \tag{2.5}$$

where Δr is the range step. Applying an *n*-term rational function to approximate the exponential function will transform Eq. (2.5) to:

$$p(r + \Delta r, z) = exp(ik_0 \Delta r)\prod_{j=1}^{n}\frac{1 + \alpha_{j,n}X}{1 + \beta_{j,n}X}p(r,z) \tag{2.6}$$

This Padé approximation consists of a sum of *n* rational-linear terms defined by the complex coefficients, $\alpha_{j,n}$ and $\beta_{j,n}$. For further details we refer to Collins (1993,1999a) and pages 460 and 463-465 in Jensen et al. (2011). The depth operator, X, is discretised using the finite-differences scheme described in Collins and Westwood (1991). UAS solves the parabolic approximation using a forward-marching finite difference scheme to solve the acoustic field in discretised steps of range and depth.

As stated earlier, the one-way wave equation requires specification of both initial and boundary conditions for the ocean environment considered. Establishing initial data for the parabolic equation involves a specification of the complex pressure over depth at the starting range of the computation transect. A self-starter is an accurate and efficient approach for obtaining an initial condition (starting field). The self-starter developed by Collins (1992, 1999b) is obtained by solving a boundary-value problem involving the PE

depth operator (hence the name) with a forcing delta function, $\delta(z - z_0)$. The self-starter for a point source is of the form:

$$p(r_0, z) = exp\left(ik_0 r_0 (1 + X)^{1/2}\right)\left(k_0^{1/2}(1 + X)^{1/4}\right)^{-1}\delta(z - z_0) \quad (2.7)$$

The sea surface is treated as a pressure-release (zero pressure) boundary, since the density of the air is much smaller than that of the water. The boundary condition is implemented in the numerical solution scheme.

UAS accounts for range-dependent change in speed of sound in the water column and bathymetry. The composition of the seafloor is treated in terms of a number of constant-density layers of sediments. UAS includes propagation in the seabed, but only handles compressional waves and not shear waves, i.e. ocean bottom sediments are modelled as fluids. The geo-acoustic profile for each soil layer includes compressed wave speed and compressional attenuation. Besides accounting for attenuation constants in the bottom layers, it is important to include density changes at the water-bottom interface as well as within the bottom itself for a realistic treatment of bottom effects on propagation. The lower boundary condition involves termination of the physical solution domain by an artificial absorption layer of several wavelengths thickness so as to ensure that no significant energy is reflected from the lower boundary. The attenuation is increased linearly over the lower few wavelengths of the grid.

UAS provides the option to include volume attenuation in the water column using the empirical model by (Francois & Garrison 1982b; Francois & Garrison 1982a). The details are described in the next section.

2.1 Water Attenuation Loss

2.1.1 Absorption Coefficient of Water

In the model of Francois-Garrison (Francois and Garrison, 1982a and 1982b), the absorption coefficient is decomposed into three terms, corresponding to the contributions of boric acid, magnesium sulphate and pure water (Lurton, 2010):

$$\alpha_{att} = A_1 P_1 \frac{f_1 f^2}{f_1^2 + f^2} + A_2 P_2 \frac{f_2 f^2}{f_2^2 + f^2} + A_3 P_3 f^2 \quad (2.8)$$

where α_{att} is the attenuation in dB/km and f is the frequency in kHz.

The contribution of boric acid $B(OH)_3$ is defined as:

$$A_1 = \frac{8.86}{c} 10^{(0.78pH-5)} \quad (2.9)$$

$$P_1 = 1 \quad (2.10)$$

$$f_1 = 2.8\sqrt{\frac{S}{35}} 10^{\left(4-\frac{1245}{T+273}\right)} \quad (2.11)$$

$$c = 1412 + 3.21T + 1.19S + 0.0167z \quad (2.12)$$

where pH is the pH value, z is the depth in m, S is the salinity in psu and T is the temperature in ºC.

The contribution of magnesium sulphate $Mg(SO)_4$ is defined as:

$$A_2 = 21.44\frac{S}{c}(1 + 0.025T) \tag{2.13}$$

$$P_2 = 1 - 1.37 \times 10^{-4}z + 6.2 \times 10^{-9}z^2 \tag{2.14}$$

$$f_2 = \frac{8.17 \times 10^{\left(8-\frac{1990}{T+273}\right)}}{1 + 0.0018(S - 35)} \tag{2.15}$$

The contribution of pure water viscosity is defined as:

$$P_3 = 1 - 3.83 \times 10^{-5}z + 4.9 \times 10^{-10}z^2 \tag{2.16}$$

with T ≤ 20ºC:

$$A_3 = 4.937 \times 10^{-4} - 2.59 \times 10^{-5}T + 9.11 \times 10^{-7}T^2 - 1.5 \times 10^{-8}T^3 \tag{2.17}$$

and T > 20ºC:

$$A_3 = 3.964 \times 10^{-4} - 1.146 \times 10^{-5}T + 1.45 \times 10^{-7}T^2 - 6.5 \times 10^{-10}T^3 \tag{2.18}$$

2.1.2 Implementation of Water Attenuation Loss

The attenuation loss in water is neglected in the paper by Collins (1999a) and the wave number is defined as:

$$k = \omega/c \tag{2.19}$$

whereas UAS considers the water attenuation loss by defining the wave number as:

$$k = (1 + i\eta\beta)\omega/c \tag{2.20}$$

where i is the imaginary unit, $\eta = (40\pi \log_{10} e)^{-1}$, $\beta = \alpha_{ab} \cdot \lambda$ (α_{ab} is the absorption coefficient in dB/m, $\lambda = c/f$ is the wave length in m).

For the definition of α please refer to Eq. (2.8), ω is the circular frequency, and c is the sound speed.

2.2 Numerical Discretisation

UAS requires an equidistant computational grid in horizontal and vertical direction. A schematic of the solution domain is shown in Figure 2.1. The spatial discretisation used in the finite difference model is defined in terms of the wavelength,λ, being modelled. Hence, the simulations take into account sensitivity to frequency components to obtain an accurate numerical solution. The depth resolution is:

$$dz = \gamma\lambda \tag{2.21}$$

and the radial resolution is then defined as:

$$dr = \varphi dz \tag{2.22}$$

where γ determines the number of fractions in which the acoustic wave is resolved in the vertical direction. In the radial direction the spatial gradients are weaker compared to the vertical direction and φ is used to relax the resolution of the propagating wave.

The numerical accuracy of the solution is not only determined by the resolution of the computational grid but is also governed by the number of Padé terms in the PE approximation. Deep water situations often require a larger number of terms in Padé series due to wide-angle propagation, in order to obtain a numerical accurate solution. An increase in terms of the Padé approximation comes at an additional computational cost. Convergence tests form the basis for an accurate numerical solution. This part is automated in the UAS algorithm, building on an extensive convergence study with focus on grid resolution, Padé series expansion and depth (seabed interaction) relevant to EIA[4] applications.

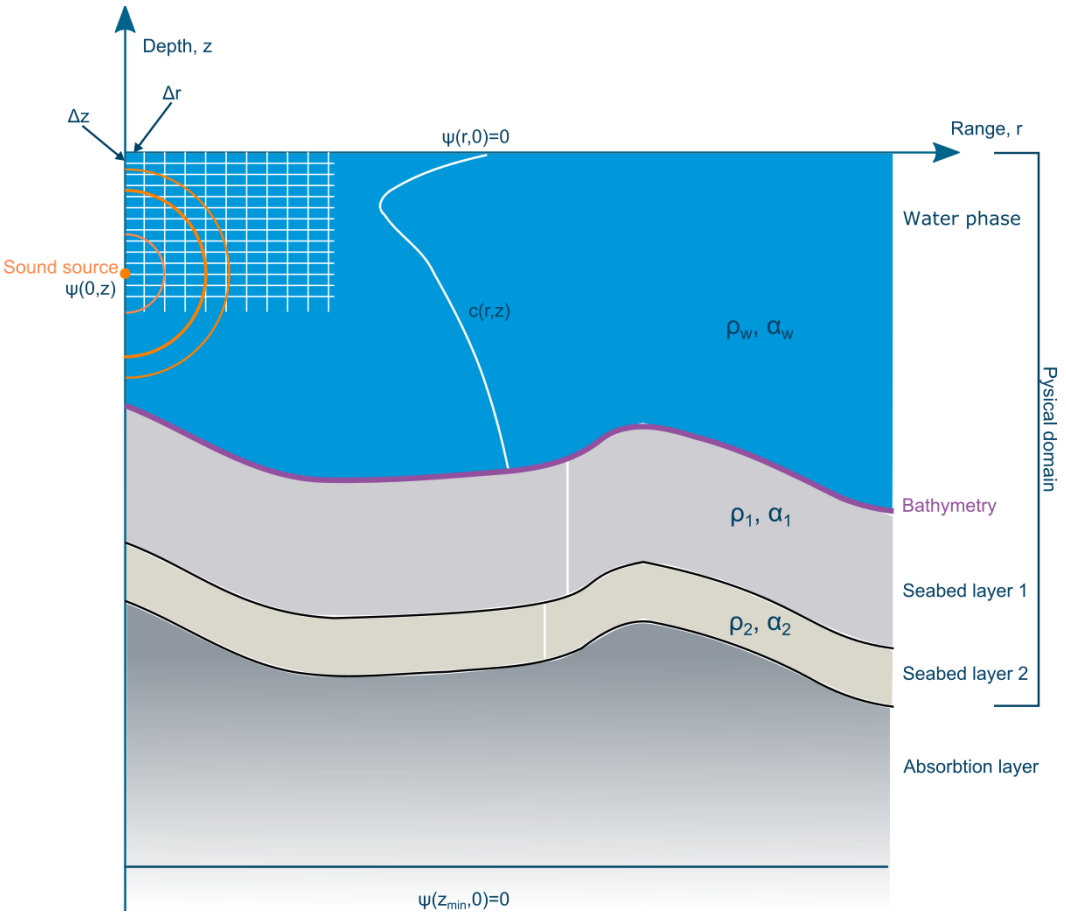

Figure 2.1 Schematic of solution domain for the UAS PE range-dependent wave propagation model

2.3 Model Assumptions

UAS is based on the following simplified conditions. The list also provides some hints to where special care must be taken in modelling of underwater sound propagation.

- The sea surface is treated as a simple, horizontal perfectly reflecting boundary ignoring the sea states, where in addition to surface gravity waves the upper ocean

[4] Environmental Impact Assessment..

will have an infusion of air bubbles which has a significant impact on the speed of sound in the surface part of the water column. It is judged that this approach will lead to conservative noise impact ranges.

  - Layers of bubbles near the surface may result in significant noise attenuation due to scattering off of surface bubble layer. Besides the enhanced transmission loss due to scattering, the sound is further attenuated by refraction caused by a spatially-varying sound velocity. Although the volume concentration of the infused air bubbles is relatively small – usually a small fraction of 1% – it has a dramatic effect on the speed of sound even for small air concentrations (Jensen et al. 2011). Particularly high-frequency acoustic propagation is highly affected by the air bubble sound attenuation mechanisms.

  - A roughness of the sea surface can be important for high frequencies (> 1 kHz).

- The impact of internal waves on sound propagation is neglected. In areas with strong stratifications the model must be used with care.

- Only compressional waves are modelled in UAS. Elastic (shear) wave propagation may be important when the bottom consists of consolidated sediments which are having enough rigidity to transmit acoustic shear waves.

  - When sound interacts with the seafloor, the structure of the ocean bottom becomes important. Ocean bottom sediments are modelled in UAS as fluids which means that they support only one type of sound wave – a compressional wave. This is often a good approximation since the rigidity (and hence the shear speed) of the sediment is usually considerably less than that of a solid, such as rock. In the latter case, which applies to the ocean basement or the case where there is no sediment overlying the basement, the medium must be modelled as elastic, which means that it supports both compressional and shear waves.

- The seabed is divided into soil layers with different acoustic properties. UAS accounts for the large-scale bathymetry, but does not resolve localised areas with large stones on the bottom or accounts for the effect of underwater sea plants on the ocean floor.

  - In shallow waters, the ocean bottom boundary condition plays a dominant role, as propagating sound waves to a larger extent interact with the ocean surface and bottom due to the short distance between the two boundaries. When sound interacts with the seafloor multiple times over short distances, the structure of the ocean bottom becomes as important as the bathymetry. Thus sound may spread significantly not only through the water but also through the underlying sediments, resulting in attenuation of its level as a result of energy being lost into the underlying sediments.

- The code is a 2D model ignoring 3D effects, due to e.g. horizontal refraction of sound rays reflected by a sloped sea bottom.

  - The seabed is in general quite flat, even close to seamounts, ridges, and the continental slopes, with a slope seldom exceeding 10o. The importance of treating the ocean bottom accurately in the numerical model depends on factors such as source-receiver separation, source frequency, and ocean depth.

  - When the seafloor is shoaling, as is the case for the ocean over a sloping beach and the continental slope, and around seamounts and islands, a ray travelling obliquely across the slope experiences the phenomenon of horizontal refraction.

- Effects of underwater ambient noise and masking are not addressed in UAS. For the most energetic part of the noise source frequencies of concern in most EIAs, the ambient level is approximately 100 dB lower, hence it is judged to have insignificantly small impact on the calculated results.
- Near-field effects are neglected. At impact ranges of interest (e.g. > 100 m), the sound intensity effects and oblique radiated sound waves dominating the near-field are to some extent diluted. The effect of the near-field on the far-field sound pressure level is EIA case dependent.

3 Validation

The Underwater Acoustic Simulator (UAS) has been successfully tested in a number of basic, idealised situations for which simulated results may be compared to analytical solutions or information from the literature.

This section presents a comparison between UAS solutions and reference solutions for two idealised cases: A deep water case (Lloyd's mirror pattern) and a shallow water case (ideal wedge).

3.1 Lloyd's Mirror Pattern

This test case simulates the acoustic interference pattern created by a point source placed near a smooth, perfectly reflecting sea surface in a deep water domain with a flat, absorbing bottom. The resulting beam pattern arises as an interference effect between the two possible sound paths from source to receiver, i.e. the direct path and the surface reflected path.

The analytical solution to the acoustic problem is (Jensen et al, 2011):

$$|\mathrm{p}| = \frac{2}{\sqrt{r^2 + {z_r}^2}} + \left|\sin\left(\frac{\mathrm{k} z_s z_r}{\sqrt{r^2 + {z_r}^2}}\right)\right|, \qquad TL = -20\log\left(\frac{|p|}{p_{ref}}\right) \tag{3.1}$$

where p is pressure, r is range, z_r is depth of the receiver, k is wave number, z_s is source depth, TL is transmission loss and p_{ref} is the reference pressure.

The model domain has a constant water depth of 5000 m and a maximum range of 30 km. In the water column a constant sound speed of 1500 m/s and an attenuation of zero are applied. In order to minimise reflections at the sea floor the bottom description comprises a bed layer with a thickness of 50 m (sound speed of 1500 m/s; density of 1200 kg/m^3; compressional attenuation of 0.5 dB/λ) and a termination layer with a thickness of 100 λ and an attenuation of 3 dB/λ, where λ is the acoustic wave length.

Two pure tone sound sources of 150 Hz and 3600 Hz placed at 25 m and 10 m water depth, respectively, were simulated.

The applied numerical settings are γ = 0.02, φ= 2, np = 5, ns = 1 and rs = 0. The mother grid (output) resolution is 1 m in the horizontal and 0.5 m in the vertical.

In Figure 3.1 the simulated transmission loss field solution for the two source frequencies is shown. In both plots the Lloyd's mirror beams (areas of low transmission loss) are clearly observed radiating from the location of the source. The number of beams, M, is found as (Jensen et al, 2011):

$$M = int\left\{\frac{2z_s}{\lambda} + 0.5\right\} \tag{3.2}$$

For the 150 Hz and 3600 Hz sources the number of beams is 5 and 48, respectively. In both plots a triangular area of irregular transmission losses is observed below the source.

Although the numerical scheme of UAS is valid for wide-angle sound propagation, these triangular areas represent source angles that are too wide (well above 60° from horizontal) for the calculated transmission losses to be accurate.

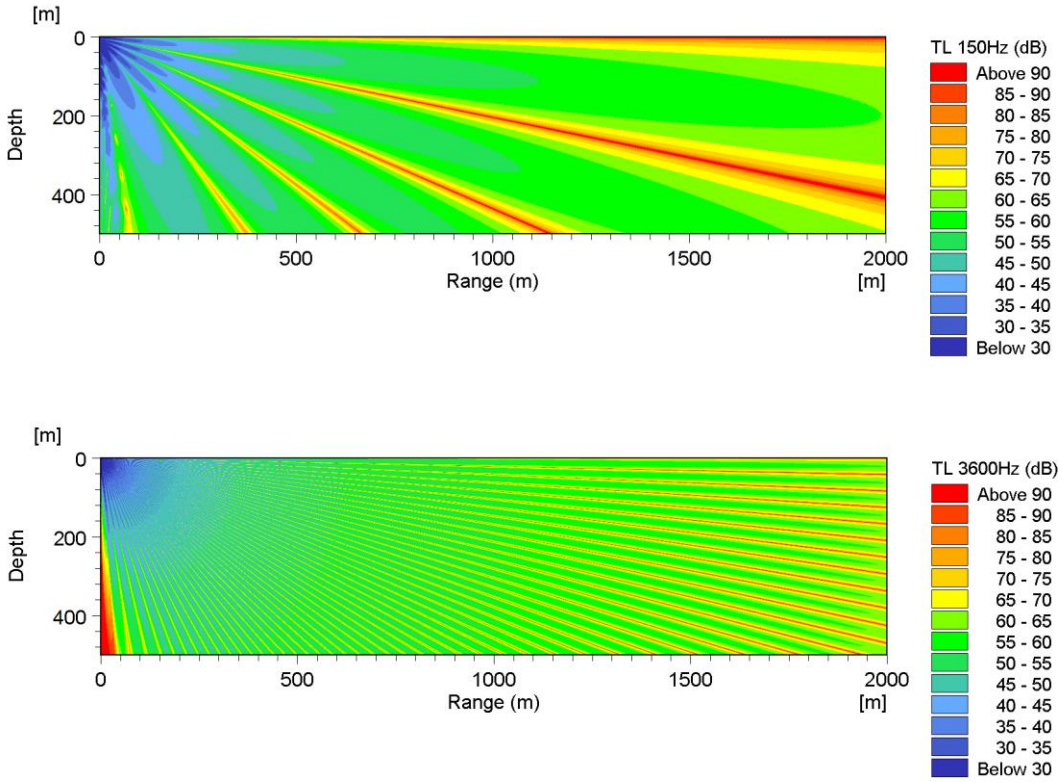

Figure 3.1 Simulated transmission loss (dB re 1 μPa^{2}s) field solutions by UAS for the Lloyd's mirror problem. The top and bottom plots show the Lloyd's mirror pattern for the 150 Hz and 3600 Hz sound sources, respectively

In Figure 3.2 comparisons between analytic and simulated transmission loss for the two sound sources at a receiver depth of 200m are shown. Also in these plots the Lloyd's mirror beams are clearly distinguishable. It is observed that the UAS results compare well to the analytic solutions for the applied source frequencies except for the first 50 m, which represent the area where the source angle is too wide for the results to be accurate. In view of UAS being a far-field propagation model the simulated results show excellent agreement with theory.

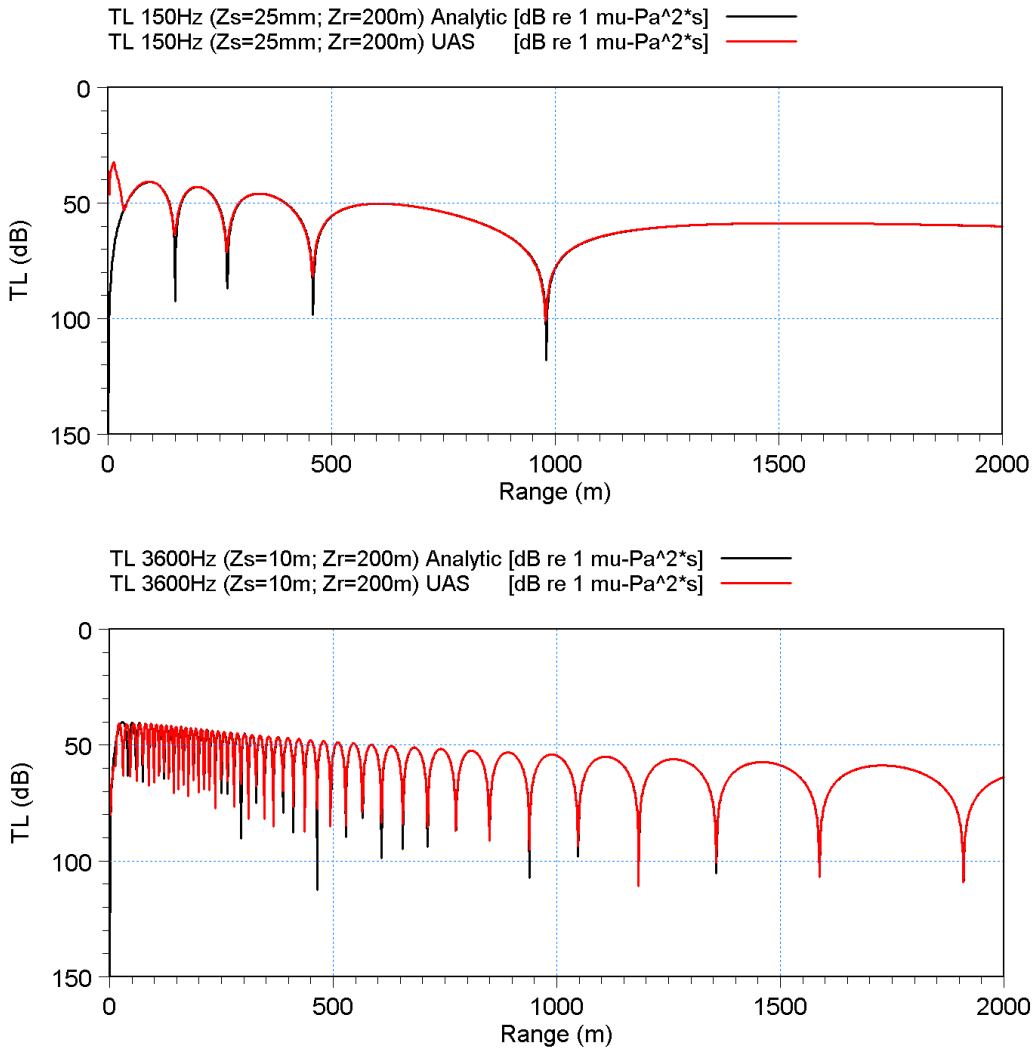

Figure 3.2 Comparison of analytic and UAS solutions for the Lloyd's mirror problem. The top and bottom plots show transmission loss at 200 m depth for the 150 Hz and 3600 Hz sources, respectively.

3.2 Ideal Wedge

The applied wedge problem is described by Jensen and Ferla (1990). The problem deals with upslope acoustic propagation in a wedge geometry with a fully reflecting, flat sea surface, a homogeneous water column (sound speed of 1500 m/s; no attenuation) and a penetrable, lossy bottom (sound speed of 1700 m/s; density of 1500 kg/m^3; compressional attenuation of 0.5 dB/λ). The water depth at the source position is 200 m decreasing linearly to 0 m at a range of 4 km. The source frequency is 25 Hz and the source depth is 100 m (mid-depth). This test configuration is referred to as "Benchmark 3" by Jensen and Ferla (1990) and is the most realistic of the benchmark wedge problems described in the paper.

In order to avoid spurious boundary reflections at the seafloor in the UAS test simulation the bottom description comprises a bed layer with a thickness of 5000 m and a termination layer with a thickness of 20 λ and an attenuation of 3 dB/λ. The applied numerical settings are γ = 0.02, φ = 5, np = 5, ns = 1 and rs = 0. The mother grid (output) resolution is 6 m in the horizontal and 1.2 m in the vertical.

In Figure 3.3 the simulated transmission loss (TL) field solution is shown down to about 285 m below the sea surface. It may be noticed in the figure that the radiation into the bottom is particularly evident at short ranges and at a range of about 3.5 km.

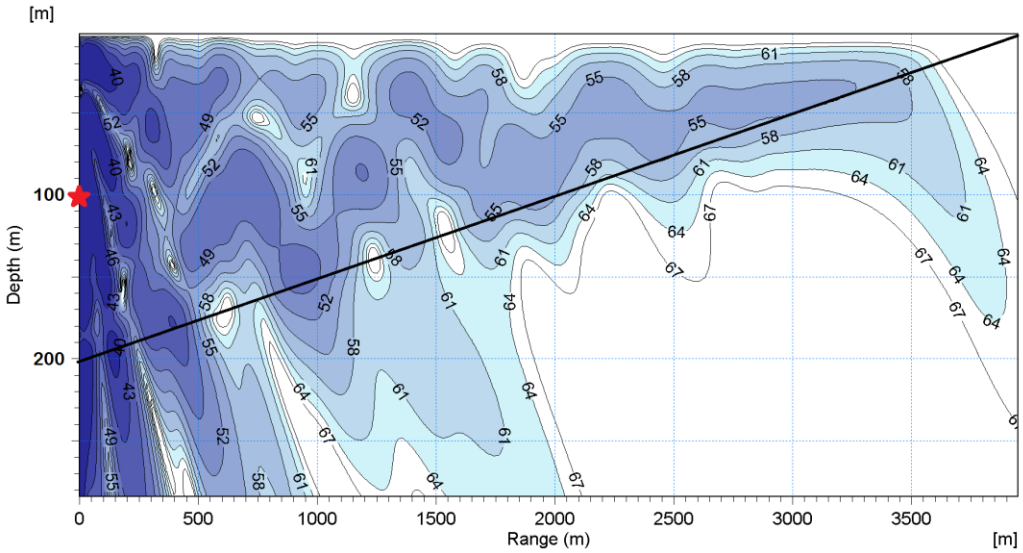

Figure 3.3 Simulated transmission loss (dB re 1 μPa^{2}s) field solution by UAS for the wedge problem with a lossy bottom. The seafloor is indicated by a black line and the location of the source by a red star

In Figure 3.4 the transmission loss at receiver depths of 30 m and 150 m is shown. Both the UAS solution and the reference solution by Jensen and Ferla (1990) are shown. It is observed in the figure that the transmission loss as simulated by UAS agrees well with the reference solution.

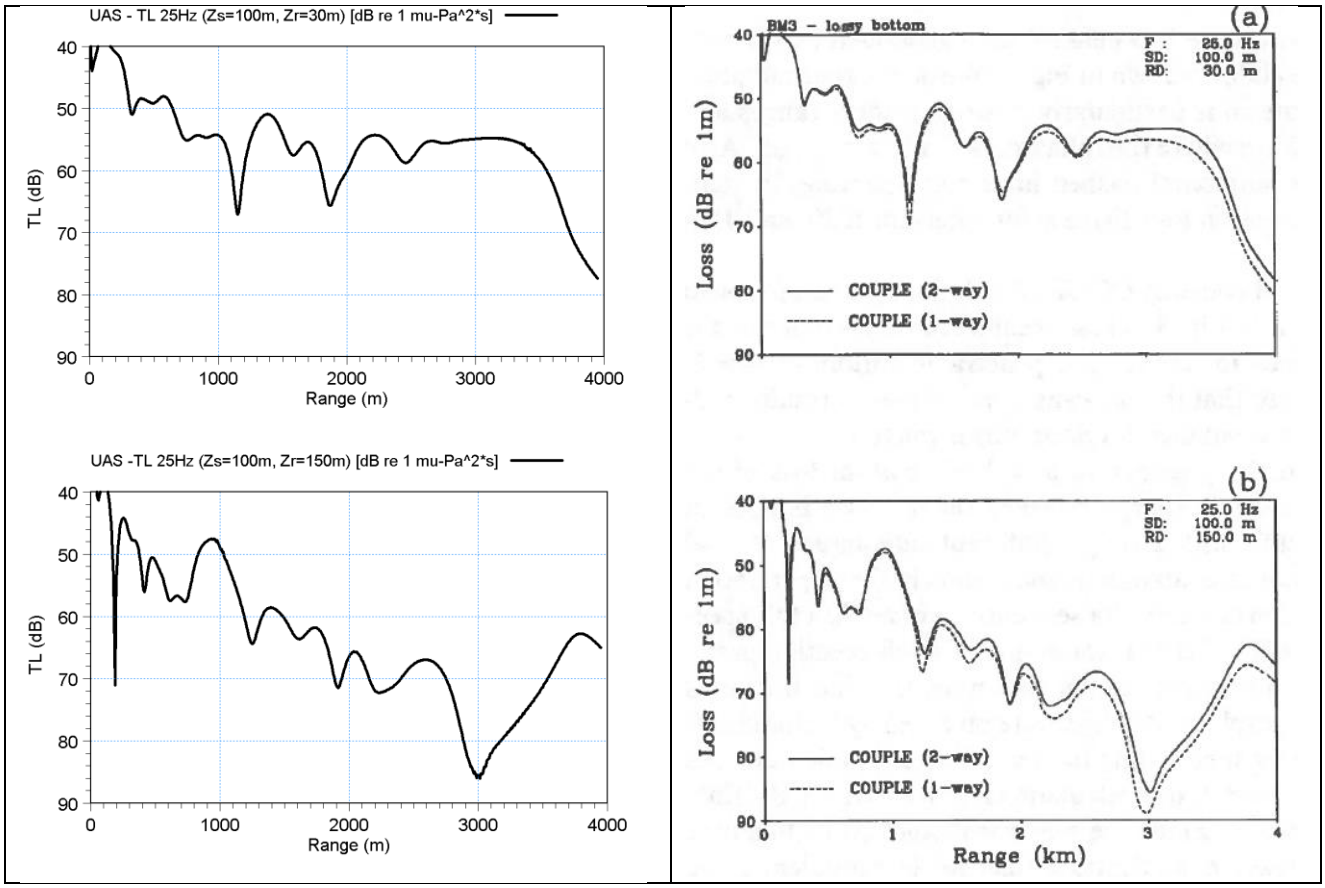

Figure 3.4 Comparison of transmission loss at 30 m and 150 m depth for the wedge problem with a lossy bottom. The left panel shows the UAS solution and the right panel (solid line) shows the reference solution (COUPLE full two-way solution) by Jensen and Ferla (1990). The paper states that the accuracy of the COUPLE (2-way) solution is within a few tenths of a decibel

4 References

Ainslie M.A. Principles of sonar performance modelling, Vol. Springer in association with Praxis Publishing Chichester, UK, 2010.

Collins, M.D. (1989). Applications and time-domain solution of higher-order parabolic equations in underwater acoustics. The Journal of the Acoustical Society of America, 86(3), 1097–1102.

Collins, M.D. and Westwood, E.K. (1991), A higher-order energy-conserving parabolic equation for range-dependent ocean depth, sound speed, and density, The Journal of the Acoustical Society of America, 89, 1068-1075.

Collins, M.D. (1992). A self starter for the parabolic equation method. J. Acoust. Soc. Am. 92, 2069–2074.

Collins, M.D., 1993. A split-step Padé solution for the parabolic equation method. Journal of the Acoustical Society of America, 93(April), pp.1736–1742.

Collins, M.D. (1999a), User's guide for RAM version 1.0 and 1.0p. http://www.siplab.fct.ualg.pt/models/ram/manual.pdf

Collins, M.D. (1999b) The stabilized self-starter. J. Acoust. Soc. Am. 106, 1724–1726.

Jensen, F.B. et al., 2011. Computational Ocean Acoustics Second edition, Springer.

Jensen F. B. and Ferla C. M. (1990) "Numerical solutions of range-dependent benchmark problems in ocean acoustics", J. Acoust. Soc. Am., Vol. 87, No. 4.

Francois, R.E. and Garrison, G.R. (1982a), Sound absorption based on ocean measurements: Part I: Pure water and magnesium sulfate contributions, Journal of Acoustical Society of America, Vol. 72 No. 3, pp. 896-907.

Francois, R.E. and Garrison, G.R. (1982b), Sound absorption based on ocean measurements. Part II: Boric acid contribution and equation for total absorption, Journal of Acoustical Society of America, Vol. 72 No. 6, pp. 1879-1890.

Lurton, X. (2010), An introduction to underwater acoustics: Principles and applications, Springer-Praxis.

Tappert, F.D. (1977). The parabolic approximation method. J. Keller and J. Papadakis, editors, Wave Propagation and Underwater Acoustics, volume 70 of Lecture Notes in Physics, pages 224–287. Springer Berlin / Heidelberg.